Rare Metal Materials and Engineering
Volume 51, Issue 1, January 2022
Available online at www.rmme.ac.cn

Science Press

Cite this article as: Zhang Xiangyun, Zhang Mi, Li Jinqi, et al. Removal Mechanism of Ni(II) from Aqueous Solution by Fe-Si-B Metallic Glass Powder[J]. Rare Metal Materials and Engineering, 2022, 51(01): 60-65.

ARTICLE

Removal Mechanism of Ni(II) from Aqueous Solution by Fe-Si-B Metallic Glass Powder

Zhang Xiangyun[1,2], Zhang Mi[1], Li Jinqi[1], Du Jinying[1], Yuan Zizhou[1]

[1] State Key Laboratory of Advanced Processing and Recycling of Nonferrous Metals, Lanzhou University of Technology, Lanzhou 730050, China; [2] Wenzhou Engineering Institute of Pump & Valve, Lanzhou University of Technology, Wenzhou 325105, China

Abstract: The commercial Fe-Si-B metallic glass (Fe-Si-B^{MG}) powder and the widely used powder of zero valent iron (ZVI), namely Fe^0, were used to eliminate the Ni(II) from aqueous solution. Kinetic analysis results indicate that the removal efficiency of Fe-Si-B^{MG} powder in removing Ni(II) is about 38 times faster than that of the Fe^0 powder. Morphology observation shows that the product layers on the surface of Fe-Si-B^{MG} powder are composed of homogeneous and loose whiskers, which peel off more easily from the surface during the agitation process, compared with those of Fe^0 powder. Chemical composition analysis about the surface of Fe-Si-B^{MG} powders before and after reaction shows that Fe-Si-B^{MG} powder can eliminate the Ni(II) through surface adsorption, reduction, and coprecipitation mechanisms; while Fe^0 powder removes the Ni(II) in solution mainly through surface adsorption and coprecipitation mechanisms.

Key words: metallic glass; reaction mechanism; activation energy; heavy metal

Enormous industry wastewater polluted by heavy metal has been discharged every year with the development of manufacturing industry[1]. Heavy metal pollution has already become a worldwide problem due to its toxicity to the plants and animals[2]. For example, the intake of Ni(II) of high concentration may cause headache, dizziness, nausea, vomiting, chest pain, tightness of the chest, dry cough, tachypnea, cyanosis, extreme weakness, and even cancer of lungs, nose and bone[3]. Therefore, great effort has been made to deal with the industrial wastewater containing heavy metal. The powder of zero valent iron (ZVI), namely Fe^0, is widely used to treat the industrial wastewater polluted by various heavy metals due to its advantages of environmental friendliness, low cost, and relatively low standard redox potential (E^0=Fe^{2+}/Fe^0=−0.44 V). For example, Ni(II) with relatively positive standard reduction potential of − 0.24 V can theoretically be reduced and adsorbed by Fe^0 powder. But the fast corrosion of Fe^0 powder leads to the rapid decrease in absorption efficiency[4]. Therefore, it is of great significance to develop the effective materials for wastewater treatment.

Recent reports showed that the Fe-based metallic glass with special atomic arrangement and metastable structure can degrade azo dyes more efficiently than Fe^0 does. It is reported that Fe-B metallic glass can degrade the tetrasodium salt (Direct Blue 6) 89 times faster than Fe^0 powder does[5]; Fe-Si-B metallic glass, namely Fe-Si-B^{MG}, can degrade tetrasodium salt and Sudanorange (Orange II) 60 and 1300 times faster than Fe^0 powder does, respectively[6-10]. Hence, the Fe-based metallic glass with special structures may eliminate the heavy metal in wastewater more efficiently.

In this research, the removal efficiency of Fe-Si-B^{MG} and Fe^0 powders in eliminating Ni(II) from aqueous solution was investigated. Additionally, the kinetic analyses and removal mechanism of the reaction process were also studied.

1 Experiment

The Fe-Si-B^{MG} powder with a nominal composition of $Fe_{78}Si_8B_{14}$ in atomic percentage was purchased from Haoxi Nano Technology Co., Ltd (Shanghai, China). The Fe^0 powder was provided with purity>99.5%. The Ni(II) solution was prepared by dissolving $NiCl_2 \cdot 6H_2O$ salt in ultra-pure water (18 MΩ·cm). Other reagents of analytical grade were used in this

Received date: January 21, 2021
Foundation item: National Natural Science Foundation of China (51661015, 52061024); Zhejiang Provincial Natural Science Foundation (LQ20E010002)
Corresponding author: Zhang Xiangyun, Ph. D., Associate Professor, State Key Laboratory of Advanced Processing and Recycling of Nonferrous Metals, Lanzhou University of Technology, Lanzhou 730050, P. R. China, E-mail: zhangxiangyun86@163.com

research.

A series of experiments were conducted by agitating 500 mg/L Ni(II) solution with a specific amount of Fe-Si-B^{MG} powder. The mixed solution was kept at a fixed temperature by water-bath method and stirred at 200 r/min. About 5 mL solution was taken out by a syringe and filtered with membrane filter of 0.2 μm at set intervals. The morphology and structure of the powders before and after reaction were analyzed by scanning electron microscopy (SEM, JSM-6700) and X-ray diffraction (XRD, Rigaku D/max-2400) with Cu Kα radiation. The concentration of Ni(II) in filtrate was analyzed via atomic absorption spectroscopy (AAS, M31-AA2600). The Brunauer-Emmett-Teller (BET) surface area analyses of the Fe-Si-B^{MG} powder and Fe^0 powder were performed using the nitrogen method with a surface analyzer model (NOVA4000). X-ray photoelectron spectroscopy (XPS) analysis was performed on the ESCALAB250 instrument with Al Kα radiation. The potential dynamic polarization curves were obtained in 100 mg/L $NiCl_2$ solution at room temperature using the CHI660E electrochemical workstation.

2 Results and Discussion

2.1 Characterization of Fe-Si-B^{MG} and Fe^0 powders

Fig. 1 shows XRD patterns of the Fe-Si-B^{MG} and Fe^0 powders. It can be seen that the XRD pattern of Fe-Si-B^{MG} powder exhibits a diffraction peak at 2θ=45° corresponding to the amorphous state, and the α-Fe phase can be observed in the XRD pattern of Fe^0 powder.

Fig. 2 shows SEM morphologies of the Fe-Si-B^{MG} and Fe^0 powders. It can be seen that all the particles are well dispersed without aggregation. Compared with the round and smooth surface of Fe-Si-B^{MG} powder (Fig. 2a), the surface of Fe^0 powder is rather irregular (Fig. 2b). Therefore, although the average diameter of Fe-Si-B^{MG} and Fe^0 powders is about 10 and 50 μm, respectively, the specific surface area (a_s) of Fe-Si-B^{MG} and Fe^0 powders measured by BET analysis is almost the same, which is 0.329 and 0.341 $m^2 \cdot g^{-1}$, respectively.

2.2 Removal efficiency

The removal efficiency of Fe-Si-B^{MG} and Fe^0 powders in removing Ni(II) from aqueous solution was investigated.

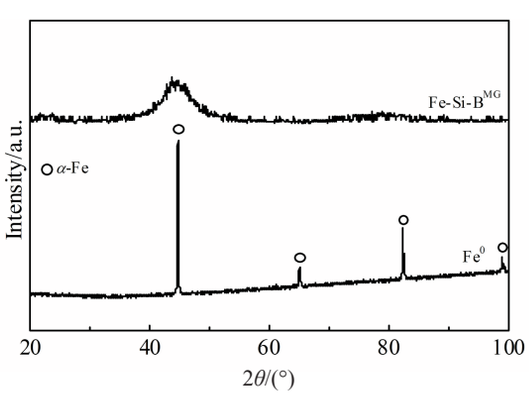

Fig.1 XRD patterns of original Fe-Si-B^{MG} and Fe^0 powders

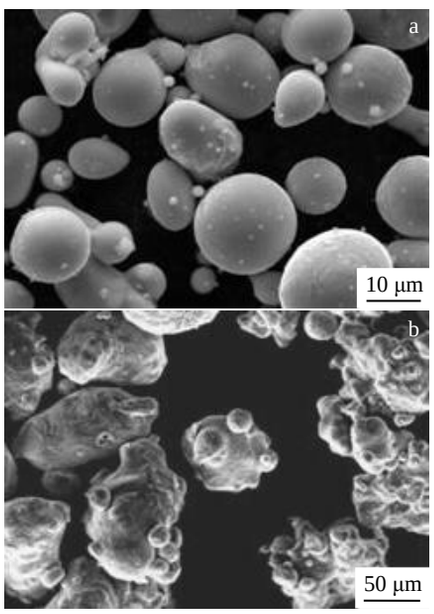

Fig.2 SEM morphologies of original Fe-Si-B^{MG} (a) and Fe^0 (b) powders

These two powders with the dosage of 3 g/L were separately put into the Ni(II) solution of 100 mg/L at 298 K. Fig.3 shows the variation of Ni(II) content after addition of Fe-Si-B^{MG} and Fe^0 powders for different durations. The removal processes of Ni(II) by Fe-Si-B^{MG} and Fe^0 powders fit well with the pseudo-first-order reaction, as expressed by Eq.(1):

$$C_t/C_0=C_1\exp(-kt)+C_2 \quad (1)$$

where C_t and C_0 are the current and initial Ni(II) content, respectively; t is the reaction time; k is the reaction rate constant; C_1 and C_2 are constants. The reaction rate constant k for Fe-Si-B^{MG} and Fe^0 powders is estimated to be 0.006 and 0.022 min^{-1}, respectively. Considering that the reaction rate is related to the specific surface area, the surface area normalized rate constant $k_{SA}=k/\rho_a$ is used to describe the interior reaction rate of the materials. ρ_a is the surface area concentration of the specimen ($\rho_a=a_s\rho_m$, where ρ_m is the mass

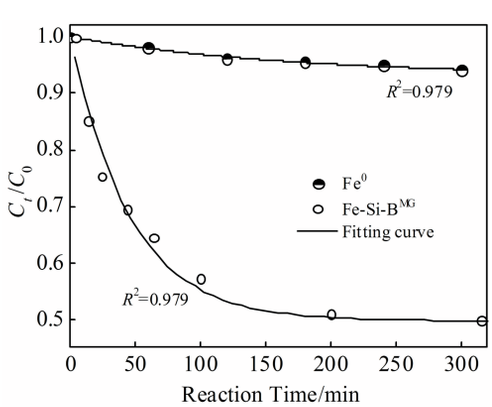

Fig.3 Relationship between C_t/C_0 and reaction time for Fe-Si-B^{MG} and Fe^0 powders

concentration of the material). The calculated k_{SA} is 0.0352 and 1.337 $L \cdot m^{-2} \cdot h^{-1}$ for Fe-Si-B^{MG} and Fe^0 powders, respectively. The reaction rate of Fe-Si-B^{MG} powder in removing Ni(II) from aqueous solution is about 38 times faster than that of the Fe^0 powders.

The reaction active energy is also a very effective parameter[11] to compare the removal efficiency of Ni(II) by Fe-Si-B^{MG} and Fe^0 powders. The removal efficiency of Fe-Si-B^{MG} and Fe^0 powders in removing Ni(II) from aqueous solution highly depends on temperature. Fig.4a shows the variation of C_t/C_0 at different temperatures of Fe-Si-B^{MG} powder, indicating that high temperature is beneficial to the reaction process between Fe-Si-B^{MG} powder and Ni(II) due to the high diffusion rate. The rate constants at different temperatures were calculated by nonlinear regression. Based on these reaction rate constants, the reaction active energy ΔE can be derived using Arrhenius-type equation, as expressed by Eq.(2):

$$\ln k = -\Delta E/RT + \ln A \quad (2)$$

where R is the gas constant, T is the temperature, and A is a constant[12]. The plots of $-\ln k$ against $1000/RT$ of the two powders are shown in Fig. 4b. The calculated reaction active energy for Fe^0 powder in removing Ni(II) from aqueous solution is 42.0 kJ/mol, indicating a surface-controlled chemical reaction (>29 kJ/mol). Nevertheless, ΔE for the Fe-Si-B^{MG} powder is 21.5 kJ/mol, indicating a diffusion-controlled reaction (8~21 kJ/mol) [13]. Since the Fe-Si-B^{MG} powder with metastable structure has a higher free energy than the thermally stable crystal solid, Fe-Si-B^{MG} powder has much lower reaction active energy than Fe^0 powder does in removing Ni(II) from aqueous solution. This result is consistent with the calculated reaction rate constants.

2.3 Reaction mechanism

The morphologies of the Fe-Si-B^{MG} and Fe^0 powders after reaction for 100 min are shown in Fig.5a and 5b, respectively. It can be seen that the Fe-Si-B^{MG} powder after reaction still keeps the spherical shape and is well dispersed without aggregation. But the Fe^0 powder becomes aggregated. It can be noticed that the reaction product peels off from Fe-Si-B^{MG}

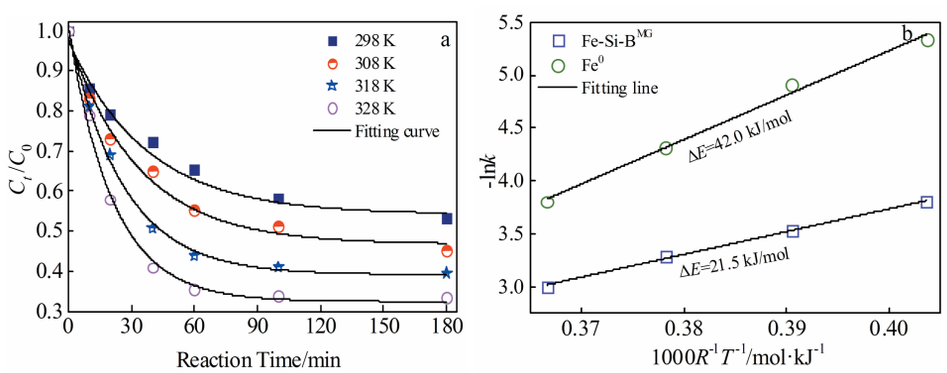

Fig.4 Relationship between C_t/C_0 and reaction time at different temperatures (a); Arrhenius plots of $-\ln k$-$1000/RT$ of removing Ni(II) by Fe-Si-B^{MG} and Fe^0 powders (b)

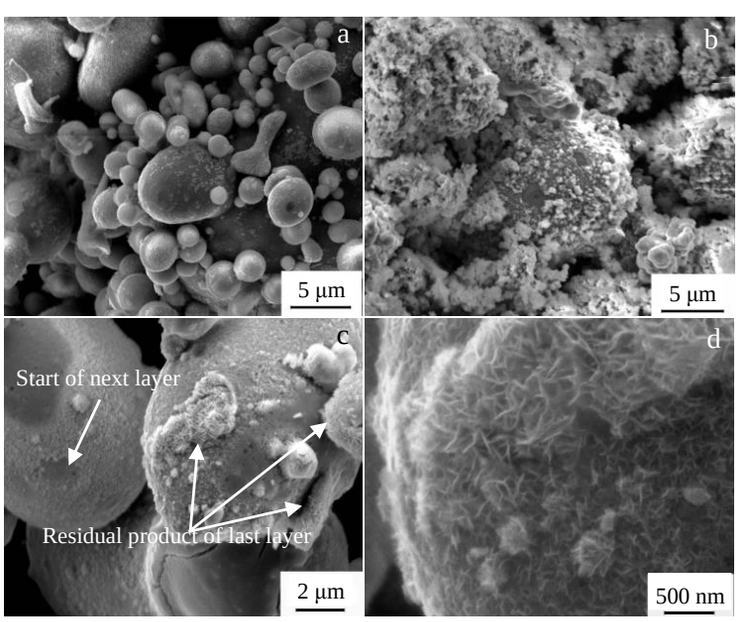

Fig.5 Surface morphologies of Fe-Si-B^{MG} (a) and Fe^0 (b) powders after reaction for 100 min; magnified morphologies of Fe-Si-B^{MG} powder (c, d)

powder layer by layer during the reaction process due to agitation. Therefore, the used particles remain their spherical shape. Fig.5c shows that some small pieces of product peel off from the powder, indicating that the next layer of product is formed and starts to peel off from the powder. At the same time, there are also some pieces of product representing the last layer which can be observed on the surface of the other powder. Furthermore, Fig. 5d shows that the product layers have homogeneous and loose porous structure consisting of numerous whiskers, which may be related to the uniform amorphous structure of metallic glass and the uniform drop style of the product layers. Interestingly, the similar morphology of product layers can also be observed in the removal process of azo dyes and Cu^{2+} from aqueous solution by amorphous alloys[14-17]. However, for the Fe^0 powder, the reaction product layers show an inhomogeneous distribution and seldomly peel off from the powders, which may be responsible for the rapid decay of its efficiency in wastewater treatment. Tang et al[5,6] studied the reaction rate of $Fe_{100-x}B_x$ (x= 16at%~20at%) amorphous ribbon, FeSiB amorphous ribbon, and their crystalline counterparts in degrading azo dye, and found that the reaction rates of amorphous ribbons are much higher than that of their crystalline counterparts. Elements B and Si contribute to the formation of an incompact product layer and can improve the degradation rate. The results are similar to the ones in this research. Therefore, it can be concluded that the formation of loose product layer on the surface of Fe-Si-B^{MG} powder is related to the Si and B elements in the powder.

Fig. 6 shows XRD patterns of Fe-Si-B^{MG} and Fe^0 powders after reaction. The Fe-Si-B^{MG} powder still retains its amorphous structure with the product layer covering the surface which is undetectable due to the low resolution of XRD analyzer. However, some diffraction peaks appear in the XRD pattern of Fe^0 powder, indicating that the product layer on the surface of Fe^0 powder is much thicker than that of Fe-Si-B^{MG} powder. This phenomenon may be related to the fact that the product layer of Fe-Si-B^{MG} powder peels off more easily from the surface than that of Fe^0 powder does.

Fig. 7 shows the potential dynamic polarization curves of pure iron ribbon, Fe-Si-B amorphous ribbon, and Fe-Si-B

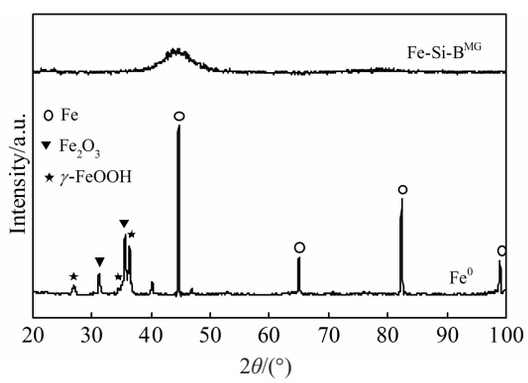

Fig.6 XRD patterns of Fe-Si-B^{MG} and Fe^0 powders after reaction

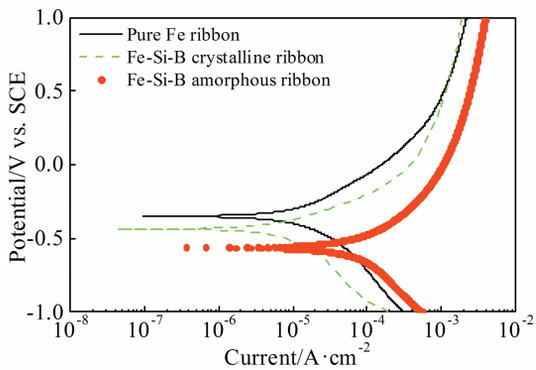

Fig.7 Polarization curves of pure iron ribbon, Fe-Si-B amorphous ribbon, and Fe-Si-B crystalline ribbon in Ni(II) solution

crystalline ribbon with the similar size. It can be seen that the Fe-Si-B amorphous ribbon has lower pitting potential and larger current density, compared with the Fe-Si-B crystalline ribbon, indicating that the Fe-Si-B amorphous ribbon is prone to corrosion in the Ni_2Cl solution[18]. According to above analysis, the high reactivity of Fe-Si-B amorphous ribbon is due to the metastable amorphous structure and low reaction active energy. Furthermore, Fe-Si-B crystalline ribbon is prone to reacting with the Ni_2Cl solution, compared with the pure Fe ribbon. Therefore, this phenomenon should be related to the formation of loose product layer of Fe-Si-B crystalline ribbon due to the addition of Si and B elements. In contrast, besides the high reaction active energy of pure Fe ribbon, the compact product layer also makes it hard to react in Ni_2Cl solution, compared with the Fe-Si-B materials.

In order to clarify the removal mechanism of Fe-Si-B^{MG} powder, the composition of Fe-Si-B^{MG} powder before and after reaction for 100 min was investigated by XPS depth analysis. Fig.8 shows XPS spectra of the Fe-Si-B^{MG} powders before and after reaction. The element composition is summarized in Table 1. It can be seen that the oxygen content in the outermost surface layer of the as-received Fe-Si-B^{MG} powder is up to 78.50at%. After the Fe-Si-B^{MG} powder was sputtered by Ar^+ for 20 s at the sputtering rate of 0.4 nm/s, the oxygen content is decreased to 3.10at% , indicating that the as-received Fe-Si-B^{MG} powder is surrounded by oxidation layer with the thickness of about 8 nm. Furthermore, the relative atomic ratio of Fe: Si: B=38.9: 35.4: 25.7 for the outermost surface layer of as-received $Fe_{78}Si_8B_{14}$ amorphous particles, indicating that Si and B are significantly enriched in the surface layer. According to Ref. [19-25], the possible components for the outmost layer of the as-received powder are: FeO_x (Fe^{2+}, 710 eV), FeOOH (712, 725.1 eV), Fe_3O_4 (713.87, 727.2 eV), Si^0 (99.2 eV), SiO (Si^{2+}, 102.28 eV), and B_xO_y (192 eV). After reaction, the surface components of the Fe-Si-B^{MG} powder change slightly into FeO_x (710.8 eV), FeOOH (712.5, 724.7 eV), Fe_3O_4 (715.2, 727.2 eV), Si^0 (99.28 eV), SiO (102.13, 101.3 eV), B_xO_y (192.2 eV), Ni^0 (852.2 eV), and Ni^{2+} (855.7 eV). But it is obvious that all the peak areas of the powder after reaction are larger than those of the as-received one,

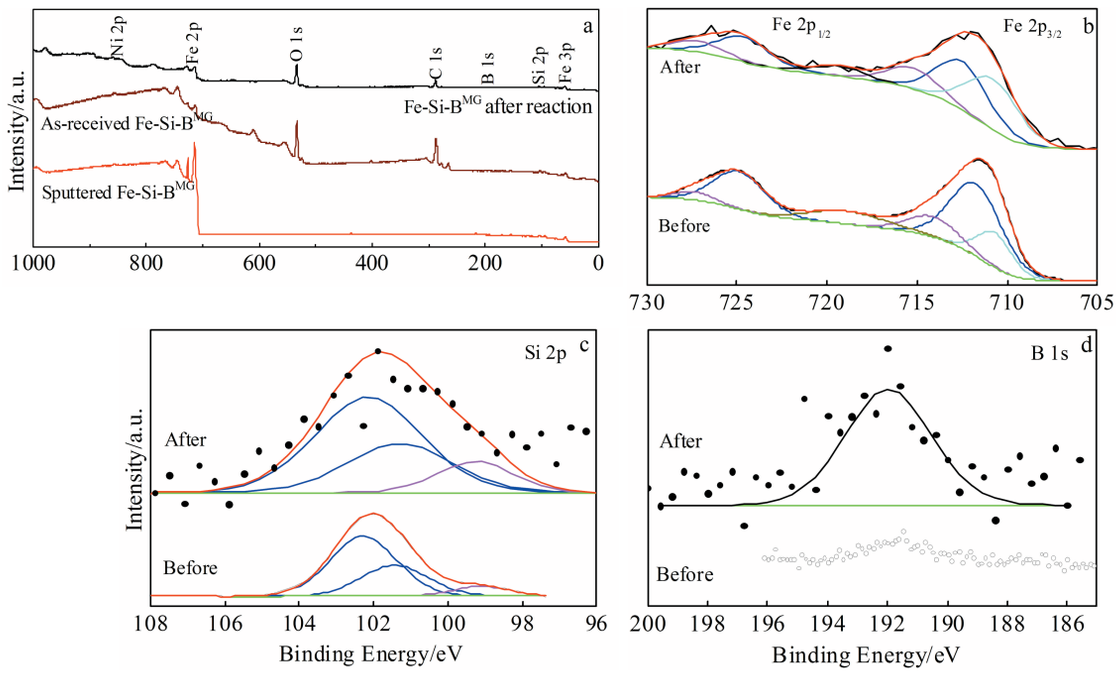

Fig.8 XPS spectra of Fe-Si-B^{MG} powders before and after reaction: (a) overall spectra, (b) Fe 2p, (c) Si 2p, and (d) B 1s

Table 1 XPS results of surface element composition of Fe-Si-B^{MG} powders before and after reaction (at%)

Specimen	Fe	Si	B	O
Before reaction	8.37	7.61	5.52	78.50
Sputtered for 20 s	77.60	6.10	13.20	3.10
After reaction	12.59	8.74	8.13	70.54

indicating that Fe, Si, and B elements are more prone to losing electrons to form oxides in $NiCl_2$ solution than in the atmosphere. These oxides peel off from the powder due to agitation and are precipitated in the solution during the reaction process.

To further explore the reaction mechanism of Fe-Si-B^{MG} powder in the solution, Ni element on the surface of the Fe-Si-B^{MG} and Fe^0 powders was detected by an advanced XPS analyzer. Fig. 9 shows XPS spectra of Ni 2p$_{3/2}$ of the two

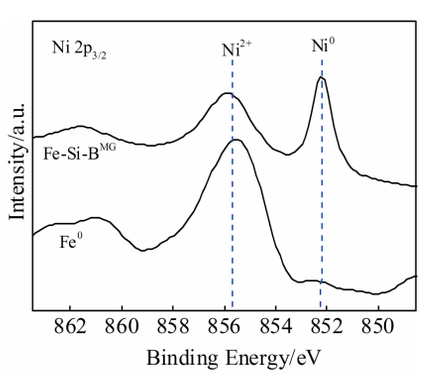

Fig.9 XPS spectra of Ni 2p$_{3/2}$ on the surface of Fe-Si-B^{MG} and Fe^0 powders

specimens. Ni^{2+} (855.8 eV) can be detected on the surface of both Fe-Si-B^{MG} and Fe^0 powders, indicating that Ni ions can combine with oxides on the surface and be removed from the solution through adsorption and coprecipitation. Furthermore, the reduced Ni^0 (852.4 eV) can be found on the surface of Fe-Si-B^{MG} powder, indicating that the initially dissolved Ni ions may gain electrons during the reaction process and the Ni^0 is precipitated on the surface of the Fe-Si-B^{MG} powder. The redox reaction can be described as follows[26]:

$$Fe^0 + Ni^{2+} \rightarrow Fe^{2+} + Ni^0 \quad (3)$$

Therefore, it can be concluded that the dissolved Ni ions in the solution is removed by Fe^0 powder mainly through the surface adsorption and coprecipitation, while Fe-Si-B^{MG} powder eliminates the Ni ions through surface adsorption, chemical reduction, and coprecipitation. Thus, Ni ions can be removed by Fe-Si-B^{MG} powder more efficiently.

3 Conclusions

1) Both the removal processes of Ni(II) by Fe-Si-B metallic glass (Fe-Si-B^{MG}) and powder with zero valent iron (Fe^0) fit well with the pseudo-first-order reaction equation. The calculated reaction constant of Fe-Si-B^{MG} powder is 38 times larger than that of Fe^0 powder; the calculated reaction active energy of Fe-Si-B^{MG} powder is smaller than that of Fe^0 powder, indicating that Fe-Si-B^{MG} powder is more efficient in removing Ni(II) ions from solution.

2) Microstructure observations show that the removal mechanism of Ni(II) in solution by Fe^0 powder is mainly surface adsorption and coprecipitation, while that by Fe-Si-B^{MG} powder is the surface adsorption, chemical reduction, and coprecipitation.

3) The product layers of Fe-Si-B^{MG} powder in Ni(II)

solution can peel off easily from the particles by agitation, which also contributes to the better reaction efficiency between Fe-Si-B^{MG} powder and Ni(II) in solution. Therefore, this work provides a new effective material for heavy metal treatment in wastewater.

References

1 Li Shaolin, Wang Wei, Liang Feipeng *et al*. *Journal of Hazardous Materials*[J], 2017, 322: 163

2 Beni A A, Esmaeili A. *Environmental Pollution*[J], 2019, 255(2): 113 298

3 Meena A K, Mishra G K, Rai P K *et al*. *Journal of Hazardous Materials*[J], 2005, 122(1-2): 161

4 Lv Z W, Yan Y Q, Yuan C C *et al*. *Materials and Design*[J], 2020, 194: 108 876

5 Tang Yao, Shao Yang, Chen Na *et al*. *RSC Advances*[J], 2015, 5(8): 6215

6 Tang Yao, Shao Yang, Chen Na *et al*. *RSC Advances*[J], 2015, 5(43): 34 032

7 Liu P, Zhang J L, Zha M Q *et al*. *ACS Applied Materials & Interfaces*[J], 2016, 6: 5500

8 Qin Xindong, Li Zhengkun, Zhu Zhengwang *et al*. *Journal of Physics and Chemistry of Solids*[J], 2019, 133: 85

9 Betancourt I, Baez S. *Journal of Non-crystalline Solids*[J], 2009, 355(22-23): 1202

10 Qin Xindong, Li Zhengkun, Zhu Zhengwang *et al*. *Journal of Materials Science & Technology*[J], 2017, 33(10): 1147

11 Wang Peipei, Wang Junqiang, Li He *et al*. *Journal of Alloys & Compounds*[J], 2017, 701: 759

12 Lv Zhuwei, Wang Weihua, Yuan Chenchen *et al*. *Materials and Design*[J], 2020, 194: 108 876

13 Lien H L, Zhang W X. *Applied Catalysis B: Environmental*[J], 2007, 77(1-2): 110

14 Chen Shuangqin, Yang Guannan, Luo Shuting *et al*. *Journal of Materials Chemistry A*[J], 2017, 5(27): 14 230

15 Chen Peng, Hu Ximei, Qi Yumin *et al*. *Metals*[J], 2017, 7(11): 485

16 Wang J Q, Liu Y H, Chen M W *et al*. *Advanced Functional Materials*[J], 2012, 22(12): 2567

17 Zhang Xiangyun, Liu Jikui, Li Jinqi *et al*. *Applied Physics A*[J], 2020, 126(4): 291

18 Ji L, Chen J W, Zheng Z G *et al*. *Journal of Physics and Chemistry of Solids*[J], 2020, 145: 109 546

19 Xie Shenghui, Peng Guangqiang, Tu Xianmeng *et al*. *Acta Metallurgica Sinica*[J], 2018, 31(11): 1207

20 Jia Zhe, Jiang Jiali, Sun Ligang *et al*. *ACS Applied Materials & Interfaces*[J], 2020, 12(40): 44 789

21 Si Jiajia, Shao Yang, Luan Hengwei *et al*. *Journal of Hazardous Materials*[J], 2020, 388: 122 043

22 Long Zhihang, Zhan Yingqing, Li Fei *et al*. *Journal of Nanoparticle Research*[J], 2017, 19(9): 318

23 Miao Shuang, An Hualiang, Zhao Xinqiang *et al*. *Reaction Kinetics, Mechanisms and Catalysis*[J], 2019, 128(1): 395

24 Sun Tao, Gong Mingfu, Cai Yuanqing *et al*. *Research on Chemical Intermediates*[J], 2020, 46(1): 459

25 Gholami P, Dinpazhoh L, Khataee A *et al*. *Journal of Hazardous Materials*[J], 2020, 381: 120 742

26 Li Shaolin, Wang Wei, Yan Weile *et al*. *Environmental Science Processes & Impacts*[J], 2014, 16(3): 524

Fe-Si-B非晶合金粉末对水溶液中Ni(II)的去除机理

张香云[1,2]，张　咪[1]，李金祺[1]，杜进英[1]，袁子洲[1]

(1. 兰州理工大学 省部共建有色金属先进加工与再利用国家重点实验室，甘肃 兰州 730050)

(2. 兰州理工大学 温州泵阀工程研究院，浙江 温州 325105)

摘　要：对比研究了商业Fe-Si-B非晶（Fe-Si-B^{MG}）粉末和目前广泛应用的零价铁粉（ZVI，Fe^0）对水溶液中重金属离子Ni(II)的去除性能。动力学分析显示Fe-Si-B^{MG}粉末对Ni(II)的去除效率约为Fe^0粉的38倍。通过对2种粉末的表面形貌观察发现，与Fe^0粉相比，Fe-Si-B^{MG}粉末的表面产物层具有均匀、疏松的絮状物，更容易在搅拌过程中脱落。通过对Fe-Si-B^{MG}粉末反应前后的表面化学成分分析发现：Fe-Si-B^{MG}粉末通过吸附、还原、共沉淀作用去除水溶液中Ni(II)，而Fe^0粉主要通过吸附和共沉淀去除水溶液中的Ni(II)。

关键词：非晶合金；反应机制；激活能；重金属

作者简介：张香云，女，1986年生，博士，副教授，兰州理工大学省部共建有色金属先进加工与再利用国家重点实验室，甘肃 兰州 730050，E-mail：zhangxiangyun86@163.com